THE JOURNAL OF BIOLOGICAL CHEMISTRY VOL. 283, NO. 45, pp. 30766–30771, November 7, 2008

Entrapment of Carbon Dioxide in the Active Site of Carbonic Anhydrase II*◆

Received for publication, July 14, 2008, and in revised form, August 15, 2008 Published, JBC Papers in Press, September 2, 2008, DOI 10.1074/jbc.M805353200

John F. Domsic[‡1], Balendu Sankara Avvaru[‡1], Chae Un Kim[§], Sol M. Gruner[§¶], Mavis Agbandje-McKenna[‡], David N. Silverman[‡‖], and Robert McKenna[‡2]

From the [‡]Department of Biochemistry and Molecular Biology and the [‖]Department of Pharmacology and Therapeutics, College of Medicine, University of Florida, Gainesville, Florida 32610 and the [§]Cornell High Energy Synchrotron Source (CHESS) and [¶]Physics Department, Cornell University, Ithaca, New York 14853

The visualization at near atomic resolution of transient substrates in the active site of enzymes is fundamental to fully understanding their mechanism of action. Here we show the application of using CO_2-pressurized, cryo-cooled crystals to capture the first step of CO_2 hydration catalyzed by the zinc-metalloenzyme human carbonic anhydrase II, the binding of substrate CO_2, for both the holo and the apo (without zinc) enzyme to 1.1 Å resolution. Until now, the feasibility of such a study was thought to be technically too challenging because of the low solubility of CO_2 and the fast turnover to bicarbonate by the enzyme (Liang, J. Y., and Lipscomb, W. N. (1990) *Proc. Natl. Acad. Sci. U. S. A.* 87, 3675–3679). These structures provide insight into the long hypothesized binding of CO_2 in a hydrophobic pocket at the active site and demonstrate that the zinc does not play a critical role in the binding or orientation of CO_2. This method may also have a much broader implication for the study of other enzymes for which CO_2 is a substrate or product and for the capturing of transient substrates and revealing hydrophobic pockets in proteins.

Since their discovery (2), the carbonic anhydrases (CAs)[3] have been extensively studied because of their important physiological functions in all kingdoms of life (3). This family of enzymes is broadly comprised of three well studied, structurally distinct families (α, β, and γ) of mostly zinc-metalloenzymes that catalyze the reversible hydration of CO_2 to bicarbonate (3, 4). More recently there have been other more distinct CAs characterized, such as a cadmium β class-mimic CA (5). However, all appear to share the same overall catalytic mechanism composed of two independent stages, shown in Equations 1 and 2, an example of a ping-pong mechanism (6, 7). In the hydration direction, the first stage is the conversion of CO_2 into bicarbonate via a nucleophilic attack on CO_2 by the reactive zinc-bound hydroxide. The resultant bicarbonate is then displaced from the zinc by a water molecule (Reaction 1).

$$CO_2 + EZnOH^- \rightleftharpoons EZnHCO_3^- \overset{H_2O}{\rightleftharpoons} EZnH_2O + HCO_3$$

REACTION 1

The second stage is the transfer of a proton from the zinc-bound water to bulk solvent to regenerate the zinc-bound hydroxide (Reaction 2). Here B is a proton acceptor in solution or a residue of the enzyme itself.

$$EZnH_2O + B \rightleftharpoons EZnOH^- + BH^+$$

REACTION 2

For hCAII (α class CA), this reaction is facilitated by a solvent molecule with a pK_a near 7 that is directly coordinated to the zinc (6). This centrally located zinc exhibits a tetrahedral configuration with three histidines (His-94, His-96, and His-119) and either a water or a hydroxide molecule. The active site cavity can be loosely described as being conical in shape having a 15 Å diameter entrance that tapers into the center of the enzyme. The cavity is partitioned into two very different environments. On one side of the zinc, deep within the active site, lies a cluster of hydrophobic amino acids (namely Val-121, Val-143, Leu-198, Thr-199-CH_3, Val-207, and Trp-209), whereas on the other side of the zinc, leading out of the active site to the bulk solvent, the surface is lined with hydrophilic amino acids (namely Tyr-7, Asn-62, His-64, Asn-67, Thr-199-Oγ_1, and Thr-200-Oγ_1) (Fig. 1*a*).

Previously, molecular dynamics studies have implied that the hydrophobic region of the active site sequesters the CO_2 substrate and orients the carbon atom in readiness for nucleophilic attack by the zinc-bound hydroxide (Reaction 1) (1, 8). Additionally, crystallographic studies have identified an ordered water molecule, positioned near the hydrophobic pocket, termed "deep water," W_{DW}, that is stabilized by the amide

* This work was supported, in whole or in part, by National Institutes of Health Grant GM25154 (to D. N. S. and R. M.) and the MacCHESS grant (National Institutes of Health Grant RR001646). This work was also supported by grants from the Thomas Maren Foundation (to R. M.), U. S. Department of Energy Grant DE-FG02-97ER62443, and CHESS, which is supported by the U. S. National Science Foundation (NSF) and National Institutes of Health-NIGMS through NSF grant DMR-0225180. The costs of publication of this article were defrayed in part by the payment of page charges. This article must therefore be hereby marked "*advertisement*" in accordance with 18 U.S.C. Section 1734 solely to indicate this fact.

◆ This article was selected as a Paper of the Week.

The atomic coordinates and structure factors (codes 3D92, and 3D93) have been deposited in the Protein Data Bank, Research Collaboratory for Structural Bioinformatics, Rutgers University, New Brunswick, NJ (http://www.rcsb.org/).

[1] Both authors contributed equally to this work.

[2] To whom correspondence should be addressed: 1600 SW Archer Rd., P. O. Box 100245, Gainesville, FL 32610. Fax: 352-392-3422; E-mail: rmckenna@ufl.edu.

[3] The abbreviations used are: CA, carbonic anhydrase; hCAII, human carbonic anhydrase II; MOPS, 3-(*N*-morpholino)-propanesulfonic acid; r.m.s.d., root mean square deviation; PDB, Protein Data Bank.

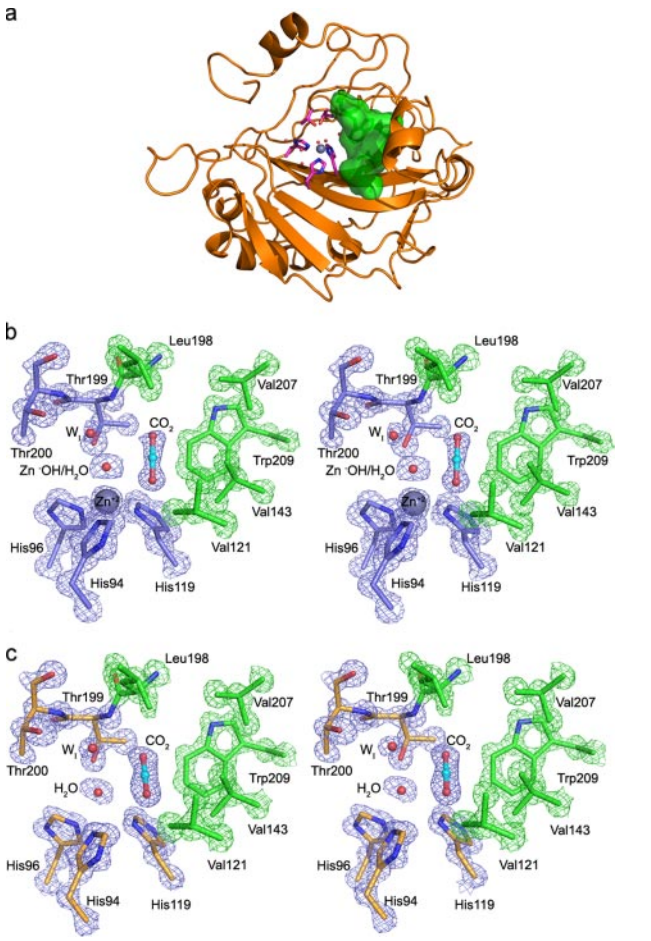

FIGURE 1. **hCAII structure.** *a*, overall view, showing the hydrophilic (*magenta stick representation*) and hydrophobic (*green surface representation*) sides of the active site. The active site zinc is shown in *purple* with the waters of the proton wire shown as *small*, *red spheres*. *b* and *c*, a close-up stereo view of the active site showing the position of bound CO_2 in holo- (*b*) and apohCAII (*c*). Electron density of the active site amino acids and W_1 (σ-weighted $2F_o - F_c$ Fourier map contoured at 2.25 σ) and CO_2 (σ-weighted $F_o - F_c$ Fourier map contoured at 2.25 σ). The figure was created using PyMOL.

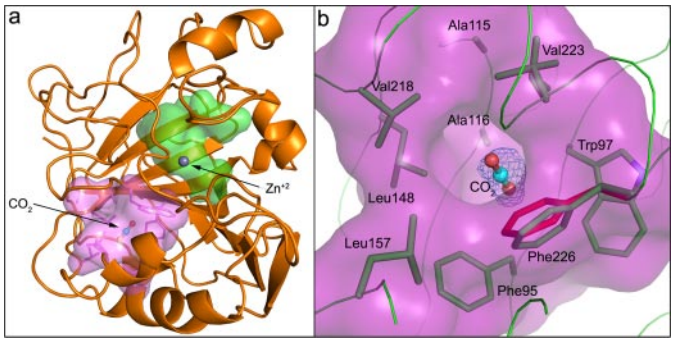

FIGURE 2. **Second CO_2 binding site.** *a*, surface representation showing the separation of the active site (*green*) and non-catalytic (*pink*) CO_2 binding pockets. *b*, close-up view of the CO_2 binding. Note the conformational change in Phe-226 (*red* = unbound, *green* = CO_2-bound holohCAII). The electron density is a σ-weighted $2F_o - F_c$ Fourier map contoured at 1.5 σ. The figure was created using PyMOL.

nitrogen of Thr-199 and the zinc-bound hydroxide (Fig. 2*a*). It has been proposed that this water is likely displaced upon the infusion of CO_2 into the binding pocket (8, 9). The hydrophilic wall of the active site has been shown, by x-ray crystallography, to create a well ordered hydrogen-bonded solvent network. It is hypothesized that this network is required to permit the transfer of a proton from the zinc-bound water to the bulk solvent via the experimentally identified proton shuttling residue His-64 (Reaction 2) (10–13). Taken together, these two very different active site environments permit the sustained and rapid catalytic cycling of CO_2 to bicarbonate.

EXPERIMENTAL PROCEDURES

Protein Purification and Crystallization—hCAII was expressed in a recombinant strain of *Eshcherichia coli* (BL21(DE3)pLysS) containing a plasmid encoding the hCAII gene (14). Purification was carried out via affinity chromatography as described previously (15). Briefly, cells were enzymatically lysed with hen egg white lysozyme, and the lysate was placed onto an agarose resin coupled with *p*-(aminomethyl)-benzene-sulfonamide, an hCAII inhibitor. The protein was eluted with 0.4 M sodium azide, 100 mM Tris-HCl, pH 7.0, and the azide was removed by extensive buffer exchanging against 10 mM Tris-HCl, pH 8.0.

Preparation of Apoenzyme—The zinc from the holoenzyme was removed by incubation at 20 °C in the chelation buffer (100 mM pyridine 2,6 dicarboxylic acid, 25 mM MOPS; pH 7.0) for 8 h. The enzyme was then buffer-exchanged against 50 mM Tris-HCl, pH 7.8, to remove the chelating agent (16). The complete loss of enzyme activity was verified through kinetic studies. The enzyme activity was revived through the addition of 1 mM $ZnCl_2$, attributing the loss of activity to the absence of zinc rather than to the denaturation of the enzyme.

Crystallization and X-ray Data Collection—Crystals of holo- and apohCAII were obtained using the hanging drop vapor diffusion method (17). 10-μl drops of equal amounts of protein and precipitant were equilibrated against precipitant solution (1.3 M sodium citrate, 100 mM Tris-HCl, pH 7.8) by vapor diffusion at room temperature (~20 °C) (13). Crystals grew to ~0.2 × 0.2 × 0.5 mm in size after ~5 days.

CO_2 Binding—To capture CO_2 in the active site of hCAII, it was essential to cryo-cool the crystals under CO_2 pressure. This was achieved using the high pressure cryo-cooling method that was originally developed for crystal cryoprotection (18). The crystals were first soaked in a cryo-solution containing 20% glycerol in precipitant solution. The crystals were then coated with mineral oil to prevent crystal dehydration and loaded into the bottom of high pressure tubes. In the pressure tubes, the crystals were pressurized with CO_2 gas at 15 atm at room temperature. 25 min later, without releasing CO_2 gas, the crystals were slowly frozen over 2 min by dipping the sealed end of the pressure tubes into liquid nitrogen. During the cooling process, it was noticed that the CO_2 gas pressure gradually dropped from 15 atm to below 1 atm due to CO_2 solidification.

X-ray Diffraction Data Collection—Diffraction data were collected at CHESS, beamline A1, at a wavelength of 0.9772 Å. Data were collected using the oscillation method in intervals of 1° step on an ADSC Quantum 210 CCD detector (Area Detector Systems Corp.), with a crystal to detector distance of 65 mm. A total of 624 and 360 images were collected for the holo and apo data, respectively. Indexing, integration, and scaling were performed using HKL2000 (19). The crystals of the CO_2-bound holo- and apohCAII diffracted to 1.1 Å resolution and were processed to a completeness of 99.9% and an R_{sym} of 8.8% and a

completeness of 93.1% and an R_{sym} of 8.0%, respectively. Complete processing statistics are given in Table 1.

Structure Solution and Model Refinement—The structures of CO_2-bound holo- and apohCAII were solved in a similar manner using the program SHELXL (20). Prior to refinement, a random 5% of the data were flagged for R_{free} analysis (21). The previously determined 1.54 Å resolution crystal structure of holohCAII (PDB ID: 2CBA) (16) was stripped of all waters, the zinc, and any alternate conformers and used as the initial phasing model in a round of least squares, rigid-body refinement to 2.5 Å resolution to an R_{factor}/R_{free} of 31.3/33.2% for holo and 28.0/28.6% for apo enzyme. The data were then extended to 1.5 Å resolution, and the model was refined using conjugant gradient least squares refinement. After 20 cycles, the model and related σ-weighted electron density maps were read into the molecular graphics program Coot (22). Improperly built side chains and the zinc (in the holo structure only) were placed into their respective density, and the model was run through another round of conjugant gradient least squares refinement. Waters with positive density in the σ-weighted difference map were kept until all waters with reasonable density were built. The data sets were then extended to 1.1 Å resolution, and the final waters were built. Disorder was then modeled into the density by modeling all visible alternate conformations for both amino acid side chains and waters. Riding hydrogens were then placed on all residues except the imidazole nitrogens of the histidines. The weighting factor was then changed to 0.2 for one round followed by the use of all data for the final round. The final R_{final}/R_{free} for holo was 10.9/12.9%, and the final R_{final}/R_{free} for apo was 10.4/13.9%. Complete refinement statistics can be found in Table 1. The model geometries and statistics were analyzed by PROCHECK (23).

Additional Structural Features—There were no major changes in any amino acid atomic positions other than that mentioned for the phenyl ring of Phe-226 (due to CO_2 binding) (Fig. 2). There were a large number of dual amino acid conformations in these structures; however, this can be attributed to the near atomic resolution of the structure and not necessarily to the pressurized environment that the crystals experienced (the alternate conformations were Ile-22, Leu-47, Ser-50, Asp-52, His-64, Ser-152, Ser-217, and Val-223 for the holo, and Ile-22, His-64, Gln-103, Asp-162, Lys-172, Glu-214, Ser-217, and Val-223 for the apo structure). Many previous structural studies of hCAII have shown that His-64 occupies two conformations, termed "in" and "out." Generally it has been seen that the "in" conformation is favored, although there may be pH effects on the ratio of "in" to "out" (10, 13). In both the holoCO_2-bound and the apoCO_2-bound structures, His-64 was seen to have a preference for the "out" conformation. Due to the presence of glycerol as a cryo-protectant, a well ordered glycerol molecule was observed at the mouth of the active site cavity. The oxygens of the glycerol overlap with the positions of the waters of the proton wire, thus indicating that the glycerol might be binding advantageously due to the "out" prevalence of His-64. Interestingly this glycerol molecule is seen only in the holo enzyme. A second molecule of glycerol is seen in the same position in both the holo and the apo structures on the surface of the protein located near residues 243–245 (Fig. 3).

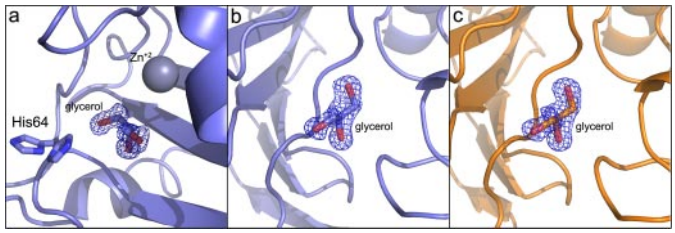

FIGURE 3. **Glycerol binding sites in CO_2-bound hCAII structures.** *a*, ordered glycerol molecule located at mouth of the active site in the holo enzyme. *b* and *c*, second ordered glycerol observed bound on the surface of the holo (*b*) and apo (*c*) structures. The electron density maps are $2F_o - F_c$ Fourier map contoured at 1.0 σ. The figure was made using PyMOL.

TABLE 1
Data and refinement statistics for CO_2-bound holo- and apohCAII

	Holo	Apo
Data collection		
Space group	P 2_1	P 2_1
Cell dimensions		
a, b, c (Å)	42.4, 41.5, 72.4	42.2, 41.5, 72.3
α, β, γ (°)	90.0, 104.1, 90.0	90.0, 104.2, 90.0
Resolution (Å)	20-1.1 (1.12-1.10)[a]	20-1.1 (1.12-1.10)
R_{sym}[b] (%)	8.8 (51.9)	8.0 (50.6)
I/σ(I)	21.0 (4.1)	35.6 (4.25)
Completeness (%)	99.9 (100.0)	93.1 (89.7)
Redundancy	11.4 (10.8)	7.0 (5.8)
Refinement		
No. Reflections	98,494	86,919
R_{factor}[c]/R_{free}[d] (%)	10.90/12.89	10.35/13.87
No. atoms		
Protein	2096	2121
Zinc/CO_2/glycerol	1/6/12	0/6/6
Water	404	352
B-factors (Å^2)		
Protein (main/side)	10.4/15.2	11.1/15.6
Zinc/CO_2[e]/glycerol	5.1/14.0, 39.5/20.1	NA/15.7, 59.7/19.1
Water	31.7	29.4
Ramachandran Plot (%)		
Allowed	89.4	88.9
Additionally allowed	10.2	10.6
Generously allowed	0.5	0.5
r.m.s.d.[f]	0.192	0.144

[a] Values in parentheses are for the highest resolution shell.
[b] $R_{sym} = (\Sigma|I - \langle I\rangle|/\Sigma\langle I\rangle) \times 100$.
[c] $R_{factor} = (\Sigma||F_o| - |F_c||/\Sigma|F_{obs}|) \times 100$.
[d] R_{free} is calculated the same as R_{factor}, except it uses 5% of reflection data omitted from refinement.
[e] The first number given is the average *B*-factor for the active site-bound CO_2, the second is for the CO_2 bound near Phe-226.
[f] The root mean square deviation of C^α positions as compared with the 1.1 Å resolution crystal structure of unbound holo hCAII (PDB ID: 2ILI) (13).

RESULTS

Here we describe for the first time, to our knowledge, the experimental capture of CO_2 in the hydrophobic cavity of hCAII (Fig. 1). The holo- and apohCAII CO_2-bound structures were refined to 1.1 Å resolution with final $R_{factors}$ of 10.90 and 10.35, respectively (Table 1). Both exhibited only minor structural perturbations when compared with the holo unbound structure (PDB ID: 2ILI) (13), with C^α r.m.s.d.s of 0.21 and 0.15 Å, respectively. The active site-bound CO_2 molecules for both the holo- and the apohCAII structures were clearly seen in the initial $F_o - F_c$ electron density maps, on the hydrophobic face of the active site, positioned within 4 Å of residues Val-121, Val-143, Leu-198, and Trp-209 (Figs. 1 and 2, Table 2) and were refined, assuming full occupancy, and had final

B-factors of 14.0 and 15.2 Å^2 (comparable with the protein), respectively (Table 1).

Comparison of holo- and apoCO_2-bound hCAII—The holohCAII structure shows, as modeled previously (1, 8), that one of the oxygens of the CO_2, O(2), interacts (3.5 Å) with the amide of Thr-199, and in doing so, causes a displacement of the water molecule W_{DW}, whereas the O(1) is positioned between the zinc and Val-121. This arrangement places both CO_2 oxygens nearly equidistant from the oxygen of the zinc-bound solvent with distances of 3.0 and 3.1 Å, respectively, putting the carbon 2.8 Å from the zinc-bound solvent. This results in a side-on orientation of CO_2 with the zinc-bound solvent, at a distance that is well suited for the nucleophilic attack to take place on the carbon by the lone pair electrons of the oxygen in the zinc-bound hydroxide (Table 2, Fig. 1*b*). Additionally, a new (or displaced) water molecule, W_1, not previously observed in other holohCAII structures is seen to occupy a space between Thr-200-Oγ_1 and the O(2) oxygen of CO_2 (Figs. 1, *b* and *c*, and 4).

Interestingly, the CO_2 molecule in the apo enzyme shares a very similar geometry despite the absence of the zinc (Fig. 1*c*). A water is positioned near what would have been the zinc-bound solvent in the holohCAII, although it is ~0.6 Å closer to the histidine ligands. Both the CO_2 oxygens are positioned ~3.1 Å from this water molecule. The small shift of this water allows the CO_2 to pivot about the O(1) atom, shifting O(2) into a slightly tighter interaction with the amide nitrogen of Thr-199 (3.15 Å for apo when compared with 3.5 Å for holohCAII) (Fig. 1, *b* and *c*).

Secondary CO_2 Binding Site—In addition to the catalytic binding site, another CO_2 binding site (not believed to be involved in catalysis) was observed in a second hydrophobic pocket, ~11 Å away from the active site (Fig. 4*a*). In this pocket, the CO_2 displaces the phenyl ring of Phe-226, inducing a 30° tilt with respect to the plane of the ring (Fig. 4*b*). Furthermore, this pocket lies next to Trp-97, a residue that biophysical analyses have shown acts as an initiator of proper folding of hCAII (24).

TABLE 2
Distance (Å) geometry of CO_2 for holo- and apohCAII
The bond distances from the CO_2 molecule are given within a radial shell of 3.9 Å. The atoms of the CO_2 molecule are in bold text. The numbering of the CO_2 oxygens are in accordance to the text and figures.

	Holo	Apo
Zinc-bound OH^-/H_2O—**C**	2.8	
*H_2O—**C**[a]		2.9
Zinc-bound OH^-/H_2O—**O(1)**	3.0	
*H_2O—**O(1)**		3.1
Zinc-bound OH^-/H_2O—**O(2)**	3.1	
*H_2O—**O(2)**		3.1
Zn^{+2}—**O(1)**	3.2	
Thr199(N)—**O(2)**	3.5	3.2
W_1—**O(2)**	3.5	3.2
His119(Nδ1)—**O(1)**	3.4	3.5
Leu198(Cα)—**O(2)**	3.4	3.5
His94(Cε1)—**O(1)**	3.3	3.2
W_1—**C**	3.6	3.2
His119(Cβ)—**O(1)**	3.5	3.6
Val121(Cγ2)—**O(1)**	3.5	3.4
Trp209(Cζ2)—**O(2)**	3.5	3.3
His94(N ε2)—**O(1)**	3.6	3.5
His119(C γ1)—**O(1)**	3.7	3.8
Leu198(Cδ2)—**O(2)**	3.7	4.1
Zn^{+2}—**C**	3.7	
Val143(C γ1)—**O(1)**	3.7	3.8
Trp209(Cη2)—**C**	3.9	3.9
Trp209(Cζ2)—**C**	3.9	3.9

[a] The water molecule in the apo hCA II is in an equivalent position to that of zinc bound OH^-/H_2O in the holo hCA II.

DISCUSSION

Catalysis of the hydration of CO_2 by hCAII at 10^8 M^{-1} s^{-1} approaches the diffusion-controlled limit and follows Michaelis kinetics with a maximal turnover near 10^6 s^{-1} and K_m near 10 mM. The diffused CO_2 is expected to be loosely bound since it has no dipole moment, and the fact that CO_2 is more soluble in organic solvents is consistent with the observed hydrophobic binding site, which suggests that solvation is a significant contributor to binding. The dissociation constant of CO_2 at the active site of hCAII was estimated by infrared spectroscopy to be 100 mM (25), a value consistent with the kinetic properties of the catalysis. The constant of Henry's Law for the solubility of CO_2 in water under the conditions of these experiments (15 atm CO_2) indicates a maximal concentration of CO_2 near 0.45 M (26). These considerations suggest a nearly complete occupancy of CO_2 at the active site.

With an energy barrier for catalysis near 10 kcal/mol, an insignificant reaction rate is expected at liquid nitrogen temperature. However, in our procedure, CO_2 was introduced to the crystal at room temperature, a procedure that surely decreased the effective pH of the crystal and surrounding solvent and promoted the forma-

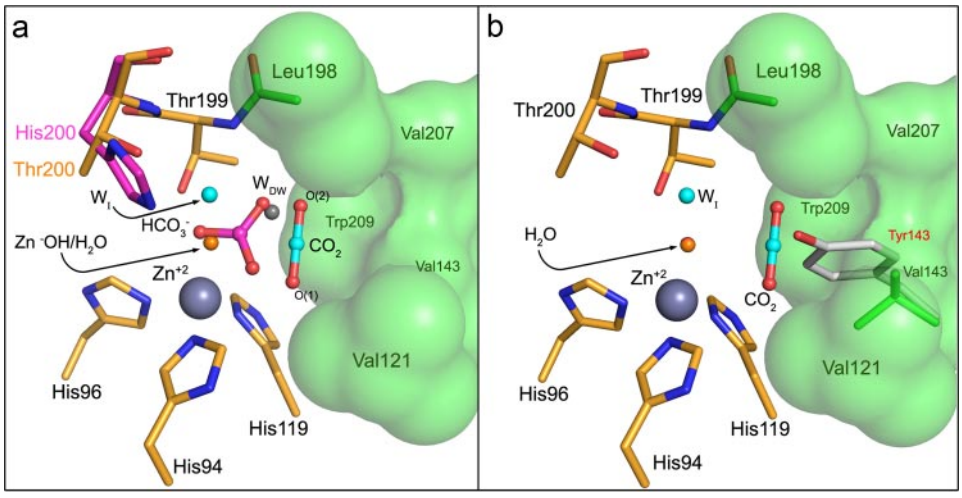

FIGURE 4. **Active site.** *a*, superposition of unbound holo- (13), CO_2-bound holo-, and bicarbonate-bound T200H hCAII (32). The binding modes of both the CO_2 substrate and the HCO_3^- product are similar, with the substrate favoring the hydrophobic side (*green*) and product favoring the hydrophilic side (*orange*). Note that the deep water (W_{DW}, *gray sphere*) is displaced and a new water occupies the area between the side chain of Thr-200 and CO_2 (W_1, *cyan*) upon CO_2 binding. The CO_2 is orientated so that the carbon is primed for the nucleophilic attack by the zinc-bound hydroxide (*orange sphere*). *b*, a superposition of the V143Y variant of hCAII (9, 27). Note that the side chain of Tyr-143 (*white*) acts as a steric block to the CO_2 binding site. The figure was created using PyMOL.

tion of the zinc-bound water at the active site. The observation of CO_2 at the active site is consistent with a zinc-bound water in our structures since this form would predominate at acidic pH and is unreactive toward CO_2. The zinc-bound hydroxide form of the enzyme reacts with CO_2; however, the observation of no bound bicarbonate suggests that this form of the enzyme was not prominent.

That the binding of CO_2 does not involve first-shell coordination to the zinc is consistent with previous spectroscopic studies (27, 28). Moreover, the observed CO_2 binding site confirms previous kinetic and structural analyses of mutations made at Val-143 (9, 29). From these studies, it was shown that bulkier substitutions led to significant decreases in activity. For example, a V143Y mutant had less than 0.02% the activity of the wild-type enzyme. A structural least squares superposition of V143Y with that of CO_2-bound wild-type enzyme (C^α r.m.s.d. = 0.26 Å) clearly shows that the tyrosine would directly interfere with CO_2 binding, thus blocking the substrate from binding in an orientation that is optimal for nucleophilic attack by the zinc-bound hydroxide (Fig. 2*b*).

The binding interactions of CO_2 determined here are very similar to those of the isoelectronic NCO^- ion that is a potent inhibitor of hCAII. Crystallographic analysis of the complex of NCO^- and hCAII shows that cyanate is bound on the hydrophobic surface of the active-site cavity and does not displace the zinc-bound water (30). Moreover, like bound CO_2, the cyanate ion displaces the deep water and forms a hydrogen bond with the backbone amide of Thr-199; the tetrahedral coordination about the zinc is not disturbed in the complex. The distance between the carbon of bound cyanate and the oxygen of zinc-bound water is 2.4 Å, again similar to the corresponding distance for bound CO_2. This comparison of the binding of CO_2 and the inhibitor NCO^- supports our hypothesis that the observed binding site of CO_2 (Fig. 1) is a site of productive substrate binding. It is interesting to note that in studies of Co(II)-substituted carbonic anhydrase, cyanate appears to bind directly to the zinc (31).

The observed binding site of CO_2 aids in the interpretation of the next step of catalysis, the formation and subsequent release of the product, bicarbonate. Following the nucleophilic attack, two mechanisms have been proposed for the subsequent release of the HCO_3^- ion based on the theoretical free energy calculations of CO_2/HCO_3^- intercoversion. The Lipscomb mechanism (32) propounds a monodentate Zn-HCO_3^- intermediate wherein a proton rapidly migrates from the original Zn-OH^- to one of the other two oxygen atoms of the HCO_3^- ion. The zinc in this mechanism is held in a tetrahedral coordination (Fig. 5*a*). In contrast, the Lindskog mechanism (33) proposes a bidentate Zn-HCO_3^- intermediate that requires one of the two oxygen atoms of the original CO_2 molecule to coordinate directly with zinc, resulting in a penta-coordinated metal ion held in a trigonal bipyramidal geometry (Fig. 5*b*).

In addition, physical evidence is provided by previous structural work. Xue *et al.* (34) made a T200H mutant that displayed a higher affinity for HCO_3^- ion than the wild-type enzyme, and as a consequence, were able to capture bicarbonate in the active site and study the complex using x-ray crystallography (Figs. 2*a* and 4). Least squares superposition of this structure on the wild-type hCAII CO_2-bound structure (C^α r.m.s.d. = 0.21 Å)

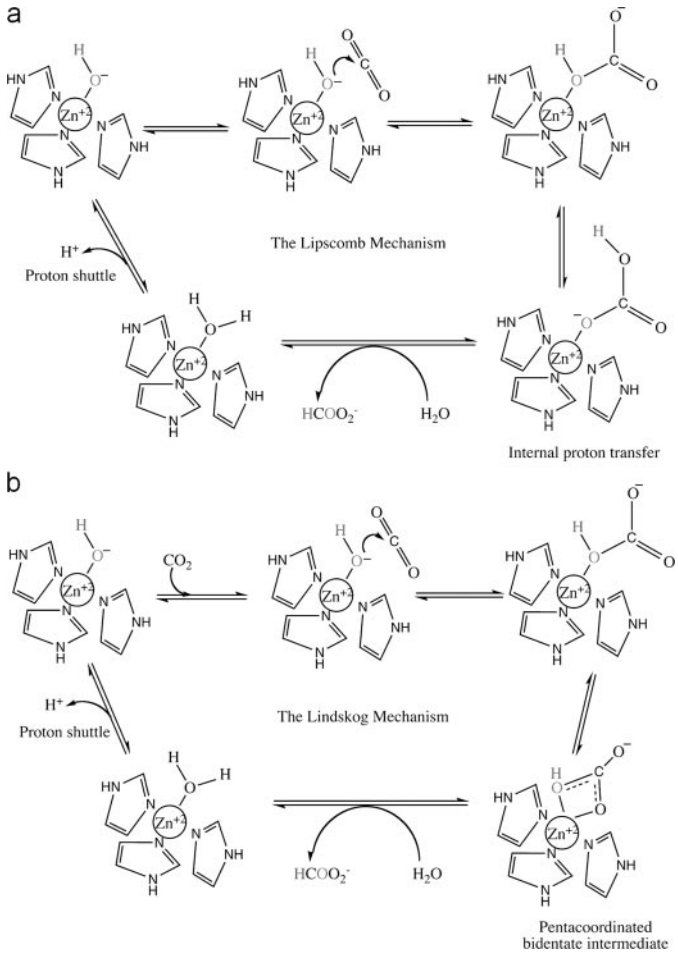

FIGUR 5. **Proposed mechanisms of hCAII catalysis.** *a* and *b*, Lipscomb (32) mechanism (*a*) and Lindskog (33) (*b*) mechanism.

shows that the CO_2 substrate molecule exists in the same plane as the Zn-HCO_3^- product (Fig. 2*a*). From a strictly structural perspective, the pseudo-bidentate nature of the captured Zn-HCO_3^- complex seems to favor the Lindskog hypothesis. Nevertheless, in both mechanisms, the release of the HCO_3^- product from the Zn-HCO_3^- intermediate is associated with the binding of a water molecule to the metal. The appearance of the previously unseen water, W_I, in close proximity to the zinc was observed in the CO_2 complex structures of both the holo and the apo enzymes. This water could be either the displaced W_{DW} water, seen prior to CO_2 binding (Fig. 2*a*), or a new ordered water, possibly arising due to a change in the local electrostatic environment. The position of this water with respect to the zinc leads us to suggest that this water may be the best candidate in the aforementioned water-associated displacement of product bicarbonate (Figs. 2 and 6).

In summary, this method of using pressurized gases, such as CO_2, may be applicable to other enzymes to capture weakly bound substrates and/or identify hydrophobic pockets in enzymes that might play important roles in substrate binding or protein folding. The identification of a CO_2 binding site at the active site of hCAII, in combination with the previously known bicarbonate binding site and the location of ordered water molecules, W_{DW} and W_I, should now guide molecular dynamics studies to examine the catalytic event itself and decipher

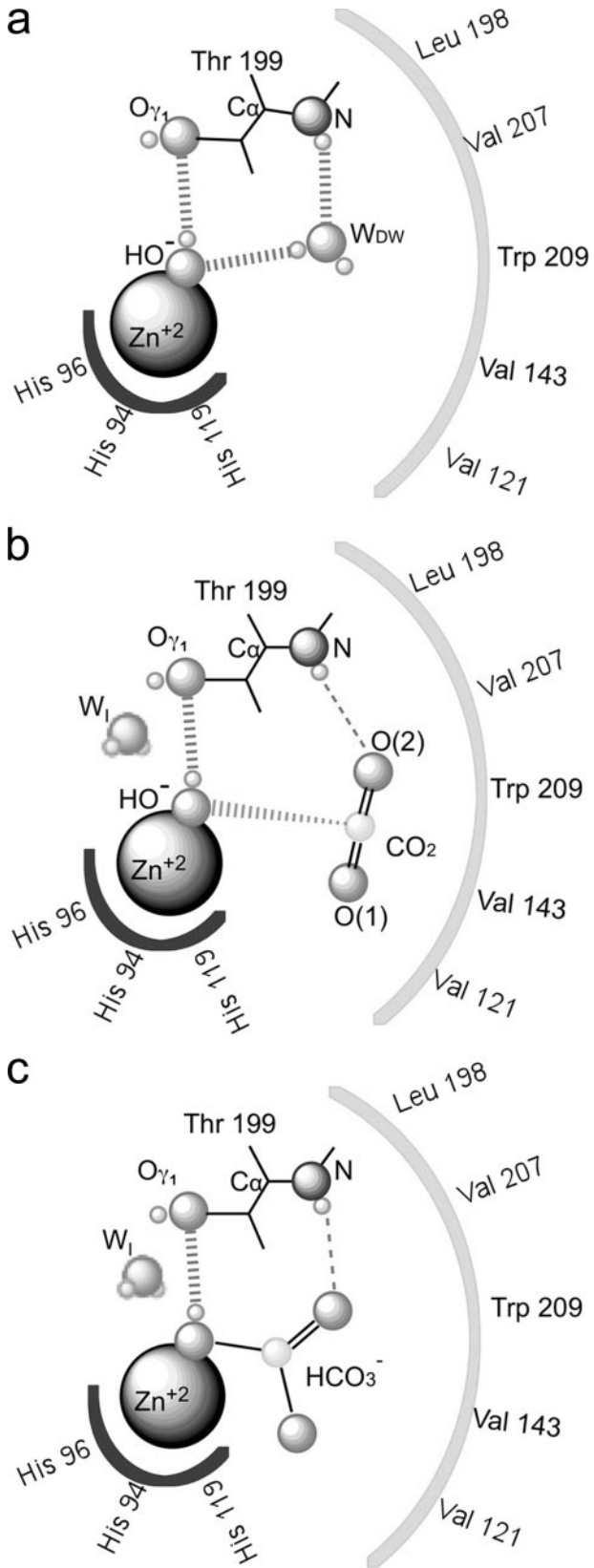

FIGURE 6. **Proposed catalytic mechanism of hCAII.** A schematic representation of three discrete stages of the catalytic cycle is shown. *a*, unbound. Note the presence of deep water (W_{DW}). *b*, CO_2 bound. Note the displacement of W_{DW} and the hydrogen bond between the substrate and backbone amide of Thr-199. *c*, the formation of bicarbonate. The figure was created using ChemDraw 11.0 (available from CambridgeSoft).

whether the Lipscomb (32) or Lindskog (33) mechanism is more feasible.

Acknowledgments—We thank Drs. Chingkuang Tu, Lakshmanan Govindasamy, and Arthur Robbins for insightful discussions.

REFERENCES

1. Liang, J. Y., and Lipscomb, W. N. (1990) *Proc. Natl. Acad. Sci. U. S. A.* **87,** 3675–3679
2. Davenport, H. W. (1984) *Ann. N Y Acad. Sci.* **429,** 4–9
3. Chegwidden, W. R., Carter, N. D., and Edwards, Y. H. (2000). *The Carbonic Anhydrases,* New Horizons, Birkhauser Verlag Basel, Switzerland
4. Christianson, D. W., and Fierke, C. A. (1996) *Acc. Chem. Res.* **29,** 331–339
5. Xu, Y., Feng, L., Jeffrey, P. D., Shi, Y., and Morel, F. M. (2008) *Nature* **452,** 56–61
6. Lindskog, S. (1997) *Pharmacol. Ther.* **74,** 1–20
7. Silverman, D. N., and Lindskog, S. (1988) *Acc. Chem. Res.* **21,** 30–36
8. Merz, K. M., Jr. (1991) *J. Am. Chem. Soc.* **113,** 406–411
9. Fierke, C. A., Calderone, T. L., and Krebs, J. F. (1991) *Biochemistry* **30,** 11054–11063
10. Silverman, D. N., and McKenna, R. (2007) *Acc. Chem. Res.* **40,** 669–675
11. Roy, A., and Taraphder, S. (2007) *J. Phys. Chem. Sect. B* **111,** 10563–10576
12. Tu, C. K., Silverman, D. N., Forsman, C., Jonsson, B. H., and Lindskog, S. (1989) *Biochemistry* **28,** 7913–7918
13. Fisher, S. Z., Maupin, C. M., Budayova-Spano, M., Govindasamy, L., Tu, C. K., Agbandje-McKenna, M., Silverman, D. N., Voth, G. A., and McKenna, R. (2007) *Biochemistry* **46,** 2930–2937
14. Forsman, C. A., Behravan, G., Osterman, A., and Jonsson, B. H. (1988) *Acta Chem. Scand. B* **42,** 314–318
15. Khalifah, R. G., Strader, D. J., Bryant, S. H., and Gibson, S. M. (1977) *Biochemistry* **16,** 2241–2247
16. Hakansson, K., Carlsson, M., Svensson, L. A., and Liljas, A. (1992) *J. Mol. Biol.* **227,** 1192–1204
17. McPherson, A. (1982) *Preparation and Analysis of Protein Crystals,* 1st Ed., Wiley, New York
18. Kim, C. U., Kapfer, R., and Gruner, S. M. (2005) *Acta Crystallogr. Sect. D Biol. Crystallogr.* **61,** 881–890
19. Otwinowski, Z., and Minor, W. (1997) *Methods Enzymol.* **276,** 307–326
20. Sheldrick, G. M. (2008) *Acta Crystallogr. Sect. A* **64,** 112–122
21. Brunger, A. T. (1992) *Nature* **355,** 472–475
22. Emsley, P., and Cowtan, K. (2004) *Acta Crystallogr. Sect. D Biol. Crystallogr.* **60,** 2126–2132
23. Laskowski, R. A., MacArthur, M. W., Moss, D. S., and Thornton, J. M. (1993) *J. Appl. Cryst.* **26,** 283–291
24. Jonasson, P., Aronsson, G., Carlsson, U., and Jonsson, B. H. (1997) **36,** 5142–5148
25. Krebs, J. F., Ippolito, J. A., Christianson, D. W., and Fierke, C. A. (1993) *Biochemistry* **32,** 4496–4505
26. Butler, J. N. (1982) *Carbon Dioxide Equilibria and Their Applications,* p. 15, Addison-Wesley Publishing Co, Reading, MA
27. Bertini, I., Luchinat, C., Monnanni, R., Roelens, S., and Moratal, J. M. (1987) *J. Am. Chem. Soc.* **109,** 7855–7856
28. Williams, T. J., and Henkens, R. W. (1985) *Biochemistry* **24,** 2459–2462
29. Alexander, R. S., Nair, S. K., and Christianson, D. W. (1991) *Biochemistry* **30,** 11064–11072
30. Lindahl, L., Svensson, L. A., and Liljas, A. (1993) *Proteins Struct. Funct. Bioinformat.* **15,** 177–182
31. Bertini, I., Luchinat, C., Pierattelli, R., and Vila, A. J. (1992) *Inorg. Chem.* **31,** 3975–3979
32. Liang, J. Y., and Lipscomb, W. N. (1987) *Biochemistry* **26,** 5293–5301
33. Lindskog, S. (1983) in *Zinc Enzymes* (Spiro, T. G., ed) pp. 78–121, John Wiley and Sons
34. Xue, Y., Liljas, A., Jonsson, B. H., and Lindskog, S. (1993) *Proteins* **15,** 80–87

Papers of the Week

Catalysis in Motion ♦

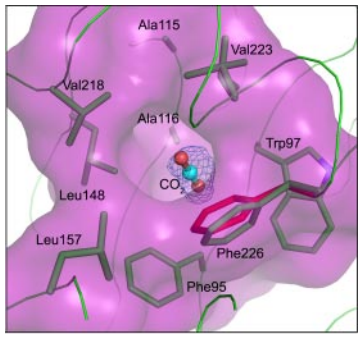

Close up view of hCAII CO_2 binding site (*red* side chain of Phe-226 represents its position in the unbound enzyme).

Visualizing enzymes with their bound substrates is fundamental to fully understand the catalytic process. In many cases, though, the substrates bind so weakly or transiently that acquiring substrate-bound forms may just be too technically daunting. In this Paper of the Week, however, John Domsic and colleagues use an innovative approach to overcome this obstacle for one such enzyme-substrate complex. They cryo-cooled crystals of human carbonic anhydrase II, which catalyzes the hydration of CO_2 to bicarbonate, under high pressure to capture the first step of this reaction. They then solved the substrate-bound structures of both the full enzyme and an apo form lacking the catalytic zinc. These structures, which do not display any major perturbations compared with the unbound enzyme, confirmed the long hypothesized binding of CO_2 in a hydrophobic pocket near the active site and also revealed that the zinc ion is not critical for proper CO_2 orientation. Domsic and colleagues believe the use of pressurized CO_2 could be useful for other CO_2-associated enzymes and perhaps even other intermediates in catalysis.

♦ See referenced article, *J. Biol. Chem.* 2008, **283,** 30766–30771